



Reconnection Rate and Transition from Ion-coupled to Electron-only Reconnection

Yundan Guan^{1,2,3}, Quanming Lu^{1,2,3}, San Lu^{1,2,3}, Kai Huang^{1,2,3}, and Rongsheng Wang^{1,2,3}¹ Deep Space Exploration Laboratory, School of Earth and Space Sciences, University of Science and Technology of China, Hefei 230026, People's Republic of China; qmlu@ustc.edu.cn, lusan@ustc.edu.cn² CAS Center for Excellence in Comparative Planetology, CAS Key Lab of Geospace Environment, Hefei 230026, People's Republic of China³ Collaborative Innovation Center of Astronautical Science and Technology, Harbin, People's Republic of China

Received 2023 June 20; revised 2023 August 24; accepted 2023 October 20; published 2023 November 23

Abstract

Standard collisionless magnetic reconnection couples with both electron and ion dynamics. Recently, a new type of magnetic reconnection, electron-only magnetic reconnection without ion outflow, has been observed, and its reconnection rate has been found to be much higher than that in ion-coupled reconnection. In this paper, using 2D particle-in-cell simulations, we find that when the ion gyroradius is much smaller than the size of the simulation domain, magnetic reconnection is standard with ion outflows. As the ion gyroradius increases, the ion response gradually weakens, and the reconnection rate becomes higher. Electron-only reconnection occurs when the ion gyroradius is comparable to the size of the simulation domain. This trend applies to both strong and weak guide field situations. Therefore, the key factor that controls the transition from ion-coupled reconnection to electron-only reconnection is the ratio between the ion gyroradius and the size of the simulation domain. We further show that, in electron-only reconnection, when the initial electron current sheet is thinner, the reconnection rate and the electron outflow speed are higher.

Unified Astronomy Thesaurus concepts: Plasma physics (2089); Space plasmas (1544); Planetary magnetospheres (997)

1. Introduction

Magnetic reconnection is an important process in space and laboratory plasma systems, and it is widely believed to be responsible for the conversion of magnetic energy to plasma energy throughout the Universe (Giovanelli 1946; Parker 1957; Sweet 1958; Biskamp 2000; Birn & Priest 2007; Yamada et al. 2010; Wang & Lu 2019; Ji et al. 2022; Lu et al. 2022). In the space environment, plasmas are usually collisionless. In collisionless magnetic reconnection, the diffusion region typically has a multiscale structure, where a small electron diffusion region is embedded in a large ion diffusion region. In the ion diffusion region, ions become demagnetized, and electrons are magnetized, which results in the Hall effect, and then ion-scale bidirectional jets are formed. In the electron diffusion region, electrons also become demagnetized and are accelerated to form electron-scale bidirectional jets (Sonnerup 1979; Ma & Bhattacharjee 1998; Birn et al. 2001; Hesse et al. 2001; Pritchett 2001; Shay et al. 2001; Fu et al. 2006; Lu et al. 2010, 2011).

Recently, electron current sheets with the currents carried mostly by electrons and the width on the order of the electron inertial length have been observed in Earth's magnetotail (Wang et al. 2018, 2020; Man et al. 2020; Hubbert et al. 2021, 2022), Earth's magnetosheath (Phan et al. 2018; Stawarz et al. 2019), the transition region of the bow shock (Gingell et al. 2020), and laboratory plasmas (Sang et al. 2022; Shi et al. 2022a, 2022b). Electron-only magnetic reconnection can occur in these thin current sheets, where only super-Alfvénic electron outflows are observed, and there are no obvious ion outflows. Electron-only reconnection may develop into standard

reconnection, in which ion outflows are formed, and therefore, it is believed to be the early stage of standard bursty reconnection (Liu et al. 2020, 2021; Lu et al. 2020b, 2022; Hubbert et al. 2022). However, electron-only reconnection observed in the magnetosheath may not evolve into the ion-coupled stage, because in the turbulent environment, the reconnecting region is too small for the ions to be coupled with the magnetic structures (Califano et al. 2020; Vega et al. 2020; Lu et al. 2021).

By performing kinetic simulations of magnetic reconnection in electron current sheets, Pyakurel et al. (2019) investigated the transition from electron-only reconnection to ion-coupled reconnection. They found that electron-only reconnection occurs when the simulation domain is smaller than 5–10 ion inertial lengths. The transition is generally gradual, and the reconnection rate decreases slowly to an asymptotic value after the ions are fully coupled. However, in their simulations, because the ion gyroradius is comparable to the ion inertial length, it is difficult to identify which one is the key factor that controls the transition.

In this paper, by performing 2D particle-in-cell (PIC) simulations, we show that the ratio between the simulation domain and the ion gyroradius is the key factor that controls the transition from electron-only reconnection to ion-coupled reconnection. Also, we find that the initial half-width of the electron current sheet influences the electron outflow speed and the reconnection rate.

2. Simulation Model

In this paper, a PIC simulation model is used. The simulations are 2.5-dimensional in the x - y plane. The initial configuration is a force-free current sheet. The initial magnetic field is $B_x = B_0 \tanh(y/\delta)$ and $B_z = \sqrt{B_0^2 + B_g^2 - B_x^2}$. Here, B_0 is the magnitude of the magnetic field for the current sheet, δ



Original content from this work may be used under the terms of the [Creative Commons Attribution 4.0 licence](https://creativecommons.org/licenses/by/4.0/). Any further distribution of this work must maintain attribution to the author(s) and the title of the work, journal citation and DOI.

Table 1
Simulation Parameters for the Runs Considered

Run	B_g/B_0	$T_e/(m_i V_A^2)$	ρ_e/d_i	$T_i/(m_i V_A^2)$	ρ_i/d_i	L/ρ_i	δ/d_i
A1	8	11.51	0.014	115.16	1.88	1.3	0.06
A2	8	11.51	0.014	27.08	0.91	2.7	0.06
A3	8	11.51	0.014	6.88	0.46	5.4	0.06
A4	8	11.51	0.014	1.69	0.23	10.8	0.06
A5	8	11.51	0.014	0.43	0.115	21.6	0.06
B1	1	0.18	0.010	28.79	5.35	0.47	0.06
B2	1	0.18	0.010	12.50	3.54	0.71	0.06
B3	1	0.18	0.010	1.80	1.34	1.86	0.06
B4	1	0.18	0.010	0.78	0.88	2.84	0.06
B5	1	0.18	0.010	0.42	0.65	3.84	0.06
C1	8	11.51	0.014	115.16	1.88	1.3	0.03
C2 (A1)	8	11.51	0.014	115.16	1.88	1.3	0.06
C3	8	11.51	0.014	115.16	1.88	1.3	0.09
C4	8	11.51	0.014	115.16	1.88	1.3	0.12
C5	8	11.51	0.014	115.16	1.88	1.3	0.15

Note. Here B_g is the guide field, T_e and T_i are the electron and ion temperatures, ρ_e is the electron gyroradius, ρ_i is the ion gyroradius, L/ρ_i is the size of the simulation domain normalized by ρ_i , and δ is the initial half-width of the electron current sheet.

is the half-thickness of the current sheet, and B_g is the uniform guide field. The magnetic fields are normalized to B_0 , density to n_0 , time to Ω_i^{-1} (where $\Omega_i = eB_0/m_i$ is the ion gyrofrequency), lengths to the ion inertial length d_i , velocities to the ion Alfvén speed V_A , electric fields to $E_0 = B_0 V_A$, and temperatures to $m_i V_A^2$. The ion gyroradius is $\rho_i = \sqrt{2m_i T_i}/(eB)$ and the electron gyroradius is $\rho_e = \sqrt{2m_e T_e}/(eB)$, where $B = \sqrt{B_x^2 + B_z^2}$. Periodic boundary conditions are used in the x -direction. Perfect conducting boundary conditions for electromagnetic fields and reflecting boundary conditions for particles are used in the y -direction.

The parameters in all the simulation cases are shown in Table 1. In Group A, the guide field $B_g = 8B_0$, while in Group B, the guide field $B_g = B_0$. In both of the groups, the size of the simulation domain is $L_x = L_y = L = 2.5d_i$, and the grid scales $\Delta x = \Delta y = 0.005d_i$. The initial current sheet is only carried by electrons. By varying the ion temperature, the ion gyroradius changes in different runs. Group C is used to study the effect of the initial half-width of the electron current sheet in electron-only reconnection. In Group C, we take Run A1 and keep all parameters unchanged, only varying the half-width of the electron current sheet.

In the simulations, the ion-to-electron mass ratio $m_i/m_e = 1836$ is used, and the speed of light $c = 300V_A$. The initial density and temperatures are uniform. Each run has 400 particles per species per grid at the initial time. A small perturbation is added to the initial magnetic flux.

3. Simulation Results

We first study the process under strong guide field conditions and use five runs (Group A) to show the transition from electron-only reconnection to ion-coupled reconnection. Figure 1 shows an overview of Run A1 and Run A5. In Run A1, due to the high ion temperature, the ion gyroradius is comparable to the size of the simulation domain, i.e., $L = 1.3\rho_i$. In this case, during the process of magnetic reconnection, the ion response is weak. As is shown in Figures 1(c) and (g), no ion outflow or ion current sheet is formed. In Figure 1(a), a quadrupolar magnetic field B_z is formed due to the in-plane electron currents in the separatrix regions (Lu et al. 2010;

Lu et al. 2011). In Figure 1(e), electron outflow can be seen clearly. The out-of-plane current is predominantly carried by the electrons, as shown in Figure 1(i).

However, in Run A5, using relatively low ion temperature, the ion gyroradius is much smaller, so the size of the simulation domain becomes larger relative to the ion gyroradius, i.e., $L = 21.6\rho_i$. In this case, the ion response in the magnetic reconnection can be obviously identified. In Figures 1(d) and (h), both an ion outflow and an ion current sheet form in the magnetic reconnection. In Figures 1(b), (f), and (j), a quadrupolar magnetic field B_z , electron outflow, and electron current sheet can also be observed. In these two simulations, the sizes of the simulation domain are the same, but due to different ion gyroradii, the degree of ion response is quite different. When the ion gyroradius is smaller, the ion response in reconnection is stronger.

Here we use the ion current density in the z -direction J_{iz} as a sign for the degree of ion response. We take cut lines for J_{iz} at $x = 0$ in all of the runs in Group A, and the result is shown in Figure 2(a). From Run A1 to Run A5, keeping the same size of the simulation domain, with the ion gyroradius becoming smaller, the ion current density becomes stronger. In Figure 2(b), the size of the simulation domain is normalized to the ion gyroradius in each run, and the trend shows that when the size of the simulation domain relative to the ion gyroradius becomes larger, the ion response becomes stronger. Because we keep the size of the simulation domain $L = 2.5d_i$ unchanged, the key factor that controls the transition from electron-only to ion-coupled reconnection is not the size of the simulation domain relative to the ion inertial length but the size relative to the ion gyroradius.

To further investigate the effect of the ion gyroradius on the ion motions in magnetic reconnection, we select two regions in the simulation domain and examine the ion velocity distribution functions therein. One region is at the x -line (yellow box in Figures 1(c) and (d)), and the other is in the outflow (green box in Figures 1(c) and (d)). For Run A1, the ion velocity distribution function at the x -line when the reconnection rate reaches its peak is shown in Figure 3(a), and the ion velocity distribution function in the outflow region is shown in Figure 3(b). Compared with the thermal velocity given by

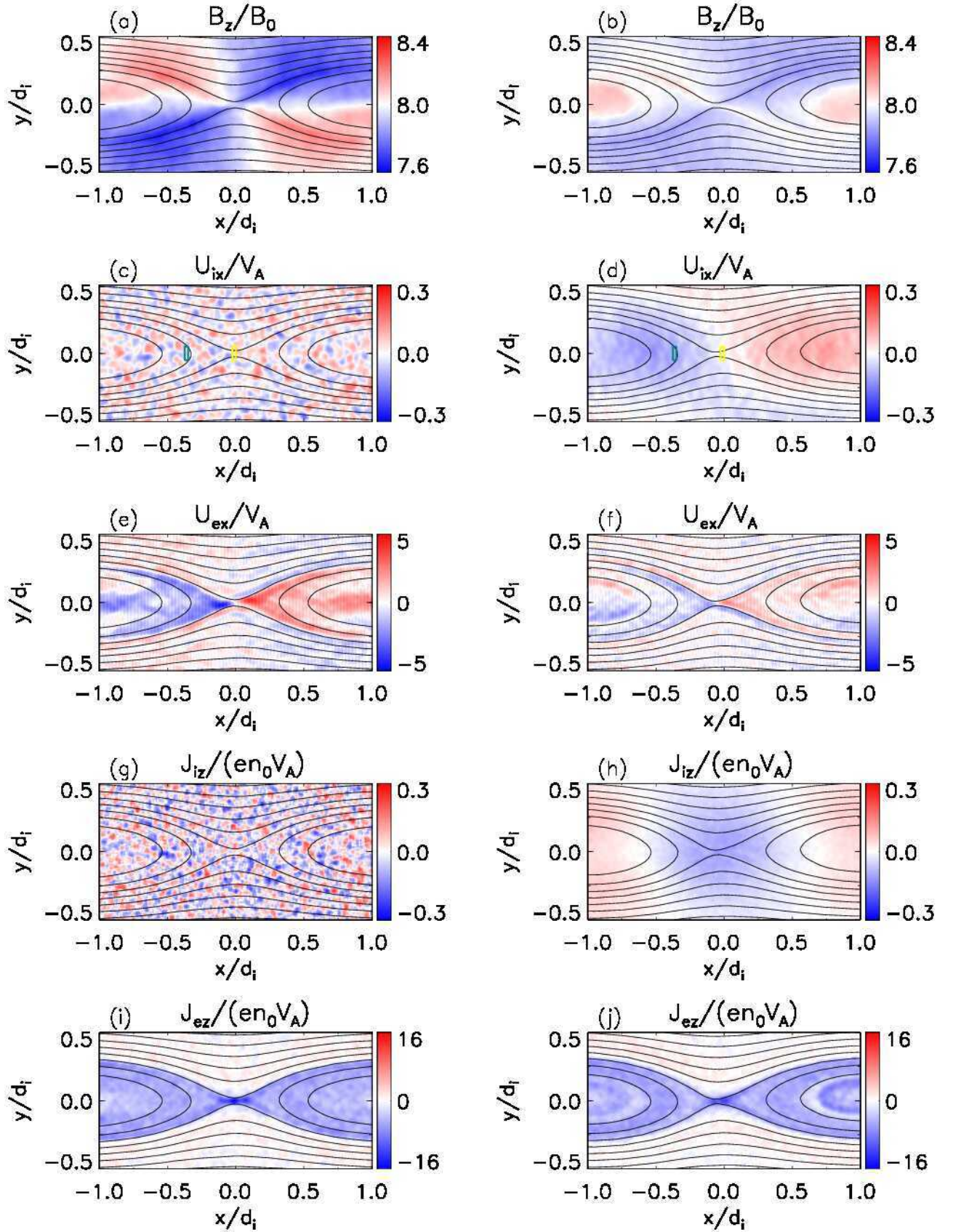


Figure 1. Overview of Run A1 (left column) at $t = 0.34\Omega_i^{-1}$ and Run A5 (right column) at $t = 0.72\Omega_i^{-1}$. (a) and (b) The Hall quadrupole magnetic field. (c) and (d) The ion bulk velocity in the x -direction. (e) and (f) The electron bulk velocity in the x -direction. (g) and (h) The ion current density in the z -direction. (i) and (j) The electron current density in the z -direction.

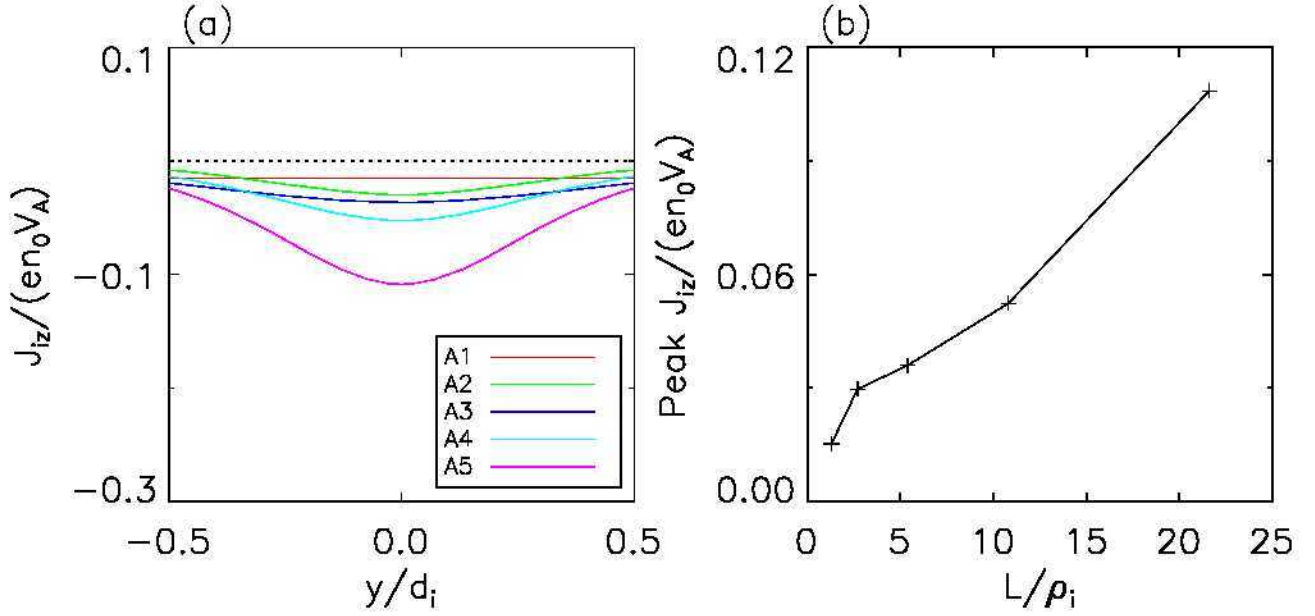


Figure 2. Overview of out-of-plane ion current density J_{iz} for all runs in Group A. (a) Cut lines of J_{iz} taken at $x = 0$ when the reconnection rate reaches its peak. The cut lines are fitted using $J_{iz} = j_{\text{peak}} \cosh^2(y/\delta)$. (b) The peak of J_{iz} vs. L/ρ_i .

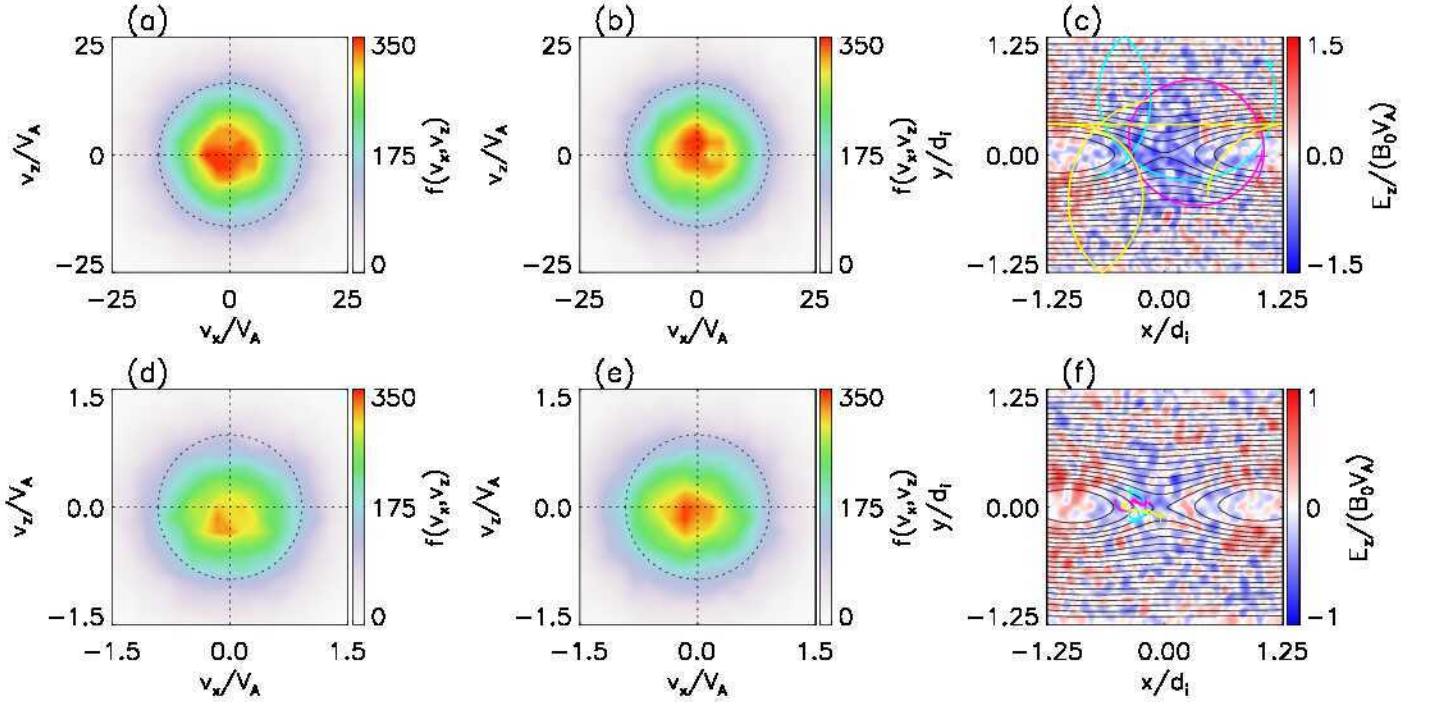


Figure 3. Ion velocity distribution functions and ion trajectories; the dashed circles in (a), (b), (d), and (e) represent the thermal velocities given by the initial ion temperatures. (a) Ion velocity distribution function in the yellow box region in Figure 1(c). (b) Ion velocity distribution function in the green box region in Figure 1(c). (c) Out-of-plane electric field E_z at $t = 0.34\Omega_i^{-1}$ and some representative ion trajectories from $t = 0$ to $t = 0.8\Omega_i^{-1}$ in Run A1. (d) Ion velocity distribution function in the yellow box region in Figure 1(d). (e) Ion velocity distribution function in the green box region in Figure 1(d). (f) Out-of-plane electric field E_z at $t = 0.72\Omega_i^{-1}$ and some representative ion trajectories from $t = 0$ to $t = 1.2\Omega_i^{-1}$ in Run A5.

the ion temperature, the velocity distribution follows the isotropic Gaussian distribution determined by the initial ion temperature. In Figure 3(c), there are several typical ion trajectories plotted over the reconnection electric field. Because of the high ion temperature in this run, the ions cross the x -line region too quickly to be accelerated, and the ion motion is mostly a gyration under the guide field with a gyroradius comparable to the size of the simulation domain. This can explain why we do not see the formation of an ion current sheet

in the z -direction, nor the formation of ion outflow in the x -direction.

For Run A5, the ion velocity distribution function at the x -line when the reconnection rate reaches its peak is shown in Figure 3(d), and the ion velocity distribution function in the outflow region is shown in Figure 3(e). In Figure 3(d), there is an obvious drift toward the $-z$ -direction, which means ions in the x -line region are accelerated by the reconnection electric field. In Figure 3(e), the drift toward the $-x$ -direction shows that

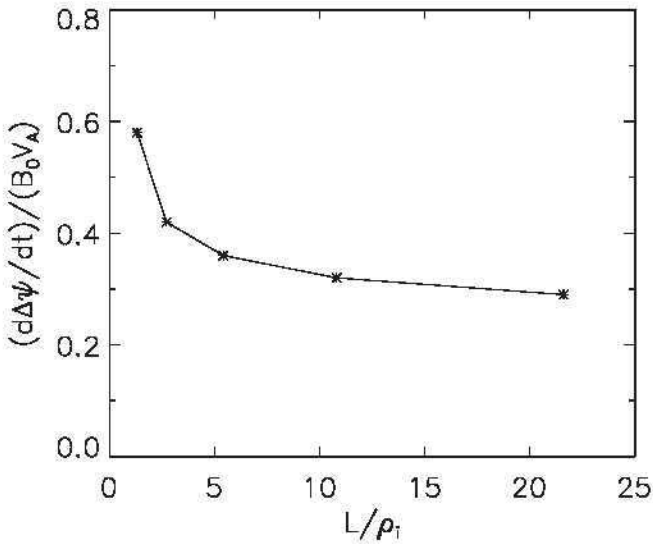


Figure 4. The maximum reconnection rate $d\Delta\psi/dt$ vs. L/ρ_i for all runs in Group A.

the accelerated ions are deflected by B_y to the $-x$ -direction and form the ion outflow. In Figure 3(f), those typical ion trajectories are no longer dominated by cyclotron motions. Relatively low thermal velocity and a small gyroradius allow the ions to stay in the x-line region for a longer time and react sufficiently to the electric field, forming the ion current sheet and ion outflow.

We use the time derivative of the magnetic flux between the x-point and the o-point to calculate the reconnection rate $d\Delta\psi/dt$, and Figure 4 shows how the maximum reconnection rate changes with the size of the simulation domain relative to the ion gyroradius. When electron-only reconnection occurs, the reconnection rate can reach $0.58B_0V_A$. By reducing the ion gyroradius, the simulation size relative to the ion gyroradius increases, the ion response becomes stronger, and the reconnection rate gradually decreases.

Then we study the process under weak guide field conditions and also use five runs (Group B) to show the transition from electron-only reconnection to ion-coupled reconnection. Figure 5 shows an overview of Run B1 and Run B5. In both runs, we observe quadrupolar magnetic fields B_z , electron outflows, and electron current sheets, as shown in Figures 5(a), (b), (e), (f), (i), and (j). In Run B1, the size of the simulation domain is $0.47\rho_i$, and there is no ion outflow in Figure 5(c). In Figure 5(g), there is only a very weak ion current sheet formed, the peak of which is $0.04en_0V_A$. Considering there is no ion outflow, and the ion current sheet density is quite weak, the response of the ions is weak enough for us to identify Run B1 as an electron-only reconnection case. In Run B5, the size of the simulation domain is $3.84\rho_i$. As is shown in Figures 5(d) and (h), ion outflow together with the ion current sheet is obviously seen. The reconnection in Run B5 is an ion-coupled reconnection.

Then we again take cut lines for J_{iz} at $x=0$ in all of the runs in Group B. The result is shown in Figure 6(a). From Run B1 to Run B5, keeping the same size of the simulation domain, with the ion gyroradius decreasing, the ion current density becomes stronger, which is consistent with the strong guide field situation. The trend is also shown in Figure 6(b).

Figure 7 shows how the maximum reconnection rate varies with the size of the simulation domain relative to the ion gyroradius under weak guide field conditions. By increasing

the ion gyroradius, the simulation size relative to the ion gyroradius decreases, the ion response becomes weaker, and the reconnection rate gradually increases. When the size of the simulation domain is $0.71\rho_i$, the reconnection rate can reach a peak, which is $0.7B_0V_A$. If we further increase the ion gyroradius (i.e., decrease the size of the simulation domain relative to it), the maximum reconnection rate does not further increase. It seems that this is the superior limit of the reconnection rate in this scenario.

Figure 8 shows the electron outflows and the reconnection rates for the runs in Group C. In this group, all of the runs have the same ion gyroradius and guide field as Run A1, so they are all electron-only reconnections without ion outflow. We find that when the initial half-thickness widens, the electron outflow speed slows down, as shown in Figures 7(a)–(c). Meanwhile, the maximum reconnection rate also decreases when the initial half-thickness widens. By thinning the width of the initial electron current, the reconnection rate in electron-only reconnection can reach $0.9B_0V_A$.

4. Conclusions and Discussion

In this paper, we study the effect of the ion gyroradius on the transition from electron-only reconnection to ion-coupled reconnection using a 2D PIC simulation model. Keeping the size of the simulation domain unchanged and varying the ion temperature, we perform a series of simulations with different ratios of the size of the simulation domain to the ion gyroradius. The results show that, for both strong and weak guide field cases, electron-only reconnection occurs when the size of the simulation domain is comparable to the ion gyroradius. As the ion gyroradius decreases, the ion response of the reconnection gradually enhances, and the reconnection rate decreases. Additionally, the reconnection rate in the electron-only runs is affected by the initial half-thickness of the electron current sheet. When the initial half-thickness of the electron current sheet is thinner, the reconnection rate and the electron outflow speed become higher.

Here we show that electron-only reconnection occurs when the ion gyroradius ρ_i is comparable to the scale of the reconnection region L . Therefore, in the regime of high ion temperature, the ions overlook the process of magnetic reconnection, which favors the occurrence of electron-only reconnection. On the other hand, according to a previous antiparallel simulation study (Ishizawa & Horiuchi 2005), ions' gyration can be disrupted when the scale length of the magnetic field $L_B(y) = B_x/(\partial B_x/\partial y)$ is smaller than the ion local gyroradius $\rho_i(y)$. The location where $L_B(y) = \rho_i(y)$ is satisfied is defined as the ion-meandering-orbit scale l_{mi} , and the ions' frozen-in constraint is broken below this scale. Similarly, the electrons' frozen-in constraint can be broken below the electron-meandering-orbit scale l_{me} . It is worth noting that in Group C, we keep the size of the simulation domain L and the ion gyroradius ρ_i the same; thus $L \sim \rho_i$ is satisfied for all runs. Meanwhile, as the half-thickness of the current sheet δ varies in Group C, the ion-meandering-orbit scale l_{mi} varies. All of the runs in Group C are electron-only reconnections without ion outflow, which implies that the occurrence of electron-only reconnection is not related to the ion-meandering-orbit scale l_{mi} , but depends on whether $L \sim \rho_i$ is satisfied. When the electron-meandering-orbit scale l_{me} varies, the electron outflow speed varies in Group C. The effect of the electron-meandering-orbit scale l_{me} on the electron outflow is expected to be important in electron-only reconnection. However, in the

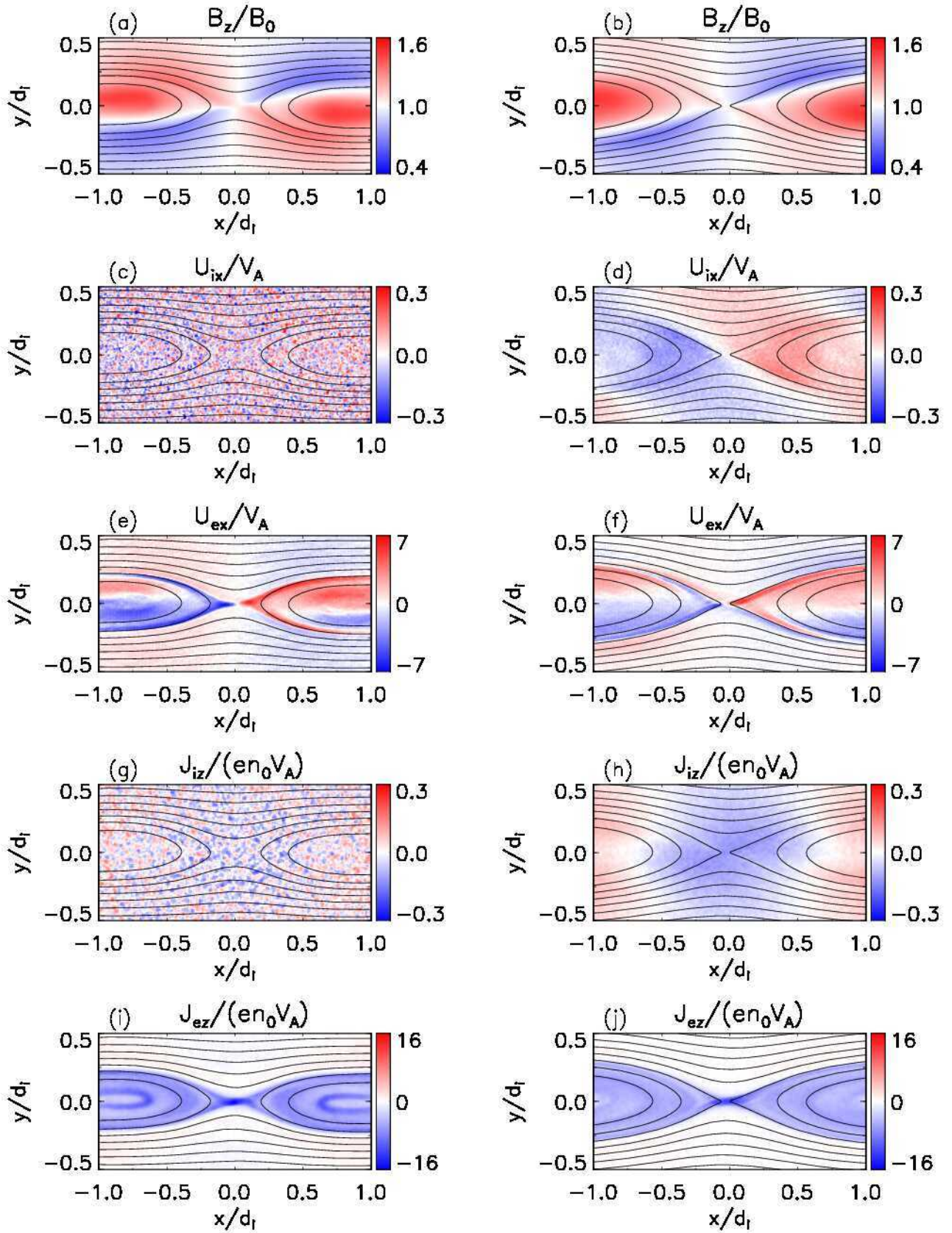


Figure 5. Overview of Run B1 (left column) at $t = 0.22\Omega_I^{-1}$ and Run B5 (right column) at $t = 0.37\Omega_I^{-1}$. (a) and (b) The Hall quadrupole magnetic field. (c) and (d) The ion bulk velocity in the x -direction. (e) and (f) The electron bulk velocity in the x -direction. (g) and (h) The ion current density in the z -direction. (i) and (j) The electron current density in the z -direction.

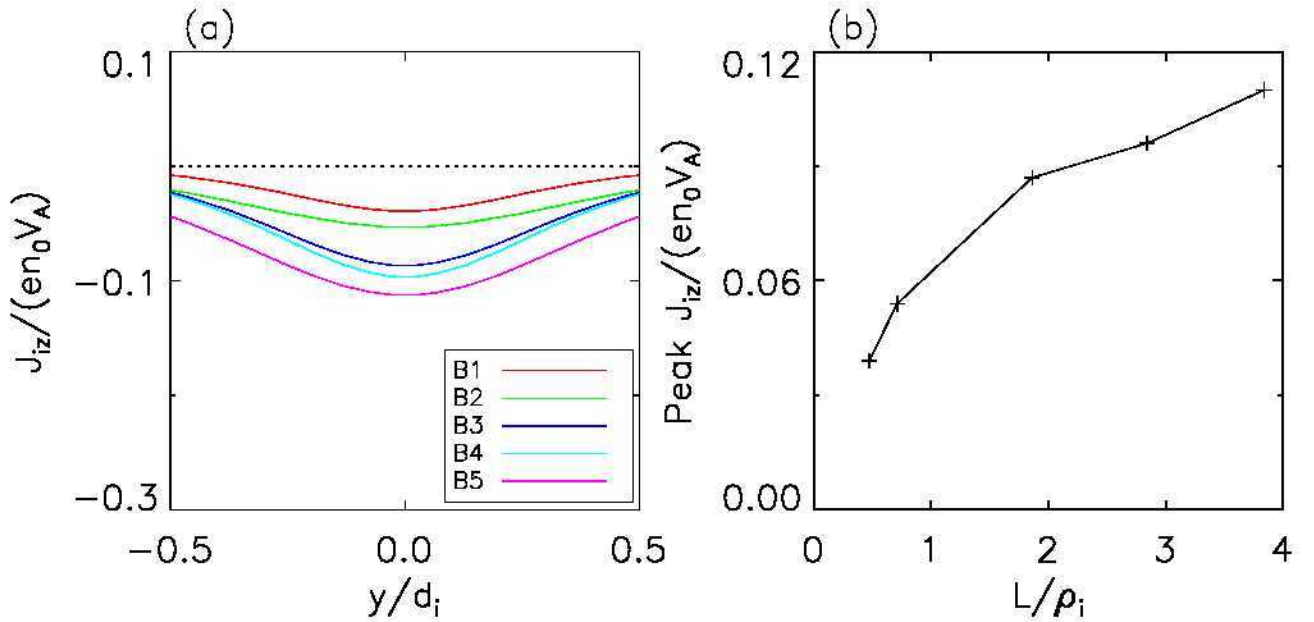


Figure 6. Overview of out-of-plane ion current density J_{iz} for all runs in Group B. (a) Cut lines of J_{iz} taken at $x = 0$ when the reconnection rate reaches its peak. The cut lines are fitted using $J_{iz} = j_{\text{peak}} \cosh^2(y/\delta)$. (b) The peak of J_{iz} vs. L/ρ_i .

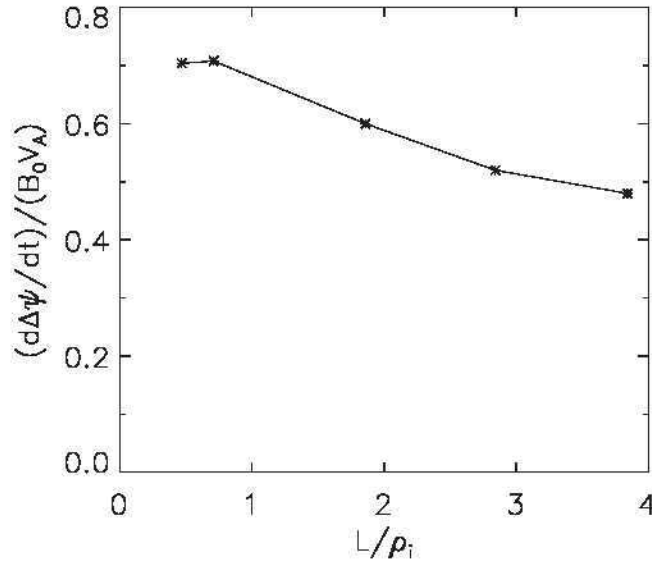


Figure 7. The maximum reconnection rate $d\Delta\psi/dt$ vs. L/ρ_i for all runs in Group B.

present study, we use a force-free current sheet with nonzero guide fields, and thus the reconnections are asymmetric, so it is not appropriate to investigate this question. To perform simulations of electron-only reconnection under antiparallel configurations, one needs a current sheet predominantly carried by electrons with an arbitrary electron-to-ion temperature ratio. The Harris current sheet dissatisfies the requirement above, and the charged current sheet model (Yoon & Lui 2004; Lu et al. 2020a) should be used in future work concerning electron-only reconnection.

Previous studies have shown that the reconnection rate in electron-only reconnection is much higher than that in standard ion-coupled reconnection. In our simulations, we show that the reconnection rate can be as high as $0.9B_0V_A$, and it is adjusted by the initial half-thickness of the electron current sheet. It should be noted that the reconnection rate here is calculated by

using the time derivative of the magnetic flux between the x-point and the o-point, and it is normalized using the asymptotic magnitude of the magnetic field B_0 and the ion Alfvén speed V_A based on B_0 and n_0 . On the other hand, recent studies using spacecraft observations (Burch et al. 2020; Pyakurel et al. 2023) and numerical simulations (Pyakurel et al. 2023) have used the electron inflow speed to represent the reconnection rate. In our study, for example, in Run B3 under the weak guide field situation, the peak electron inflow velocity $V_{ey} \sim 1.1V_A$, the local magnetic field $B_x \sim 0.4B_0$, and the local electron Alfvén speed $V_{Aex} \sim 15.5V_A$, and therefore, the electron inflow velocity is $\sim 0.07V_{Aex}$, which is consistent with the aforementioned numerical studies. In this run, the reconnection rate $(d\Delta\psi/dt)/(B_0V_A) \sim 0.47$ when it is normalized using the local V_{Aex} and B_x , i.e., $(d\Delta\psi/dt)/(B_xV_{Aex})$, is also ~ 0.07 . The reason for such a high reconnection rate in

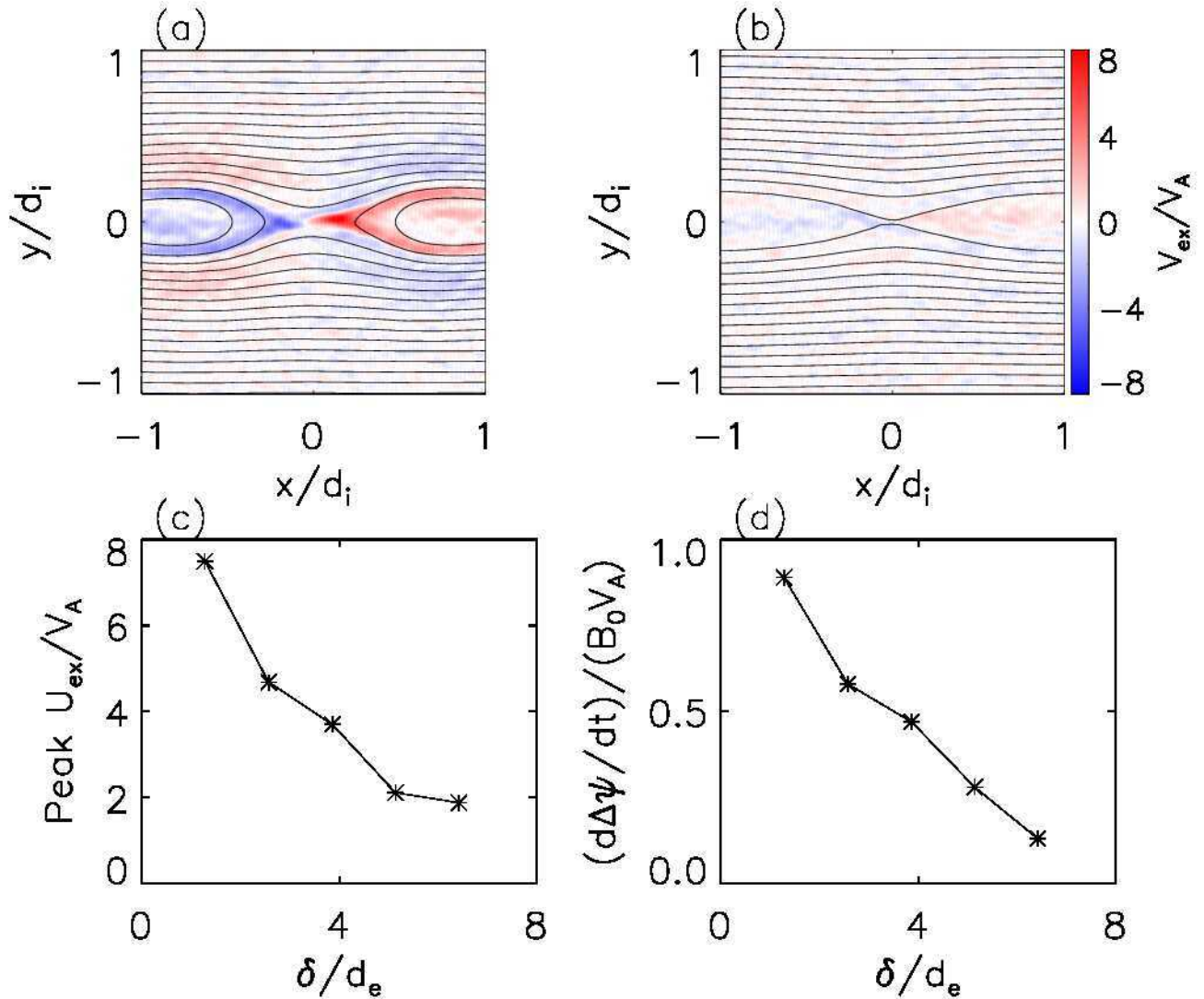


Figure 8. The electron outflow at (a) $t = 0.20\Omega_i^{-1}$ in Run C1 and at (b) $t = 0.48\Omega_i^{-1}$ in Run C5. (c) The peak of electron outflow vs. the initial half-thickness for all runs in Group C. (d) The maximum reconnection rate vs. the initial half-thickness for all runs in Group C.

electron-only reconnection is still unknown and deserves further investigation.

Acknowledgments

This work was supported by the National Key Research and Development Program of China (No. 2022YFA1604600), the NSFC grants 42174181 and 42274196, and the Strategic Priority Research Program of the Chinese Academy of Sciences, grant No. XDB 41000000.

ORCID iDs

Quanming Lu <https://orcid.org/0000-0003-3041-2682>
 San Lu <https://orcid.org/0000-0003-2248-5072>
 Kai Huang <https://orcid.org/0000-0003-3630-309X>
 Rongsheng Wang <https://orcid.org/0000-0002-9511-7660>

References

Birn, J., Drake, J. F., Shay, M. A., et al. 2001, *JGR*, **106**, 3715
 Birn, J., & Priest, E. R. 2007, *Reconnection of Magnetic Fields: Magnetohydrodynamics and Collisionless Theory and Observations* (Cambridge: Cambridge Univ. Press)

Biskamp, D. 2000, *Magnetic Reconnection in Plasmas* (Cambridge: Cambridge Univ. Press)
 Burch, J. L., Webster, J. M., Hesse, M., et al. 2020, *GeoRL*, **47**, e89082
 Califano, F., Cerri, S. S., Faganello, M., et al. 2020, *FrP*, **8**, 317
 Fu, X., Lu, Q., & Wang, S. 2006, *PhPI*, **13**, 012309
 Gingell, I., Schwartz, S. J., Eastwood, J. P., et al. 2020, *JGRA*, **125**, e27119
 Giovanelli, R. G. 1946, *Natur*, **158**, 81
 Hesse, M., Birn, J., & Kuznetsova, M. 2001, *JGR*, **106**, 3721
 Hubbert, M., Qi, Y., Russell, C. T., et al. 2021, *GeoRL*, **48**, e91364
 Hubbert, M., Russell, C. T., Qi, Y., et al. 2022, *JGRA*, **127**, e29584
 Ishizawa, A., & Horiuchi, R. 2005, *PhRvL*, **95**, 045003
 Ji, H., Daughton, W., Jara-Almonte, J., et al. 2022, *NatRP*, **4**, 263
 Liu, D., Huang, K., Lu, Q. M., et al. 2021, *ApJ*, **922**, 51
 Liu, D., Lu, S., Lu, Q. M., Ding, W., & Wang, S. 2020, *ApJL*, **890**, L15
 Lu, Q. M., Fu, H., Wang, R., & Lu, S. 2022, *ChPhB*, **31**, 089401
 Lu, Q. M., Huang, C., Xie, J., et al. 2010, *JGRA*, **115**, A11208
 Lu, Q. M., Yang, Z., Wang, H., et al. 2021, *ApJ*, **919**, 28
 Lu, S., Angelopoulos, V., Artemyev, A. V., et al. 2020a, *PhPI*, **27**, 102902
 Lu, S., Lu, Q. M., Cao, Y., et al. 2011, *ChSBu*, **56**, 48
 Lu, S., Lu, Q. M., Wang, R. S., et al. 2022, *GeoRL*, **49**, e98547
 Lu, S., Wang, R. S., Lu, Q. M., et al. 2020b, *NatCo*, **11**, 5049
 Ma, Z., & Bhattacharjee, A. 1998, *GeoRL*, **25**, 3277
 Man, H. Y., Zhou, M., Yi, Y. Y., et al. 2020, *GeoRL*, **47**, e89659
 Parker, E. N. 1957, *JGR*, **62**, 509
 Phan, T. D., Eastwood, J. P., Shay, M. A., et al. 2018, *Natur*, **557**, 202
 Pritchett, P. L. 2001, *JGR*, **106**, 3783
 Pyakurel, P. S., Phan, T. D., Drake, J. F., et al. 2023, *ApJ*, **948**, 20

- Pyakurel, P. S., Shay, M. A., Phan, T. D., et al. 2019, [PhPI](#), **26**, 082307
- Sang, L., Lu, Q. M., Xie, J. L., et al. 2022, [PhPI](#), **29**, 102108
- Shay, M. A., Drake, J. F., Rogers, B. N., & Denton, R. E. 2001, [JGR](#), **106**, 3759
- Shi, P. Y., Srivastav, P., Barbhuiya, M. H., et al. 2022a, [PhRvL](#), **128**, 025002
- Shi, P. Y., Srivastav, P., Barbhuiya, M. H., et al. 2022b, [PhPI](#), **29**, 032101
- Sonnerup, B. 1979, in *Solar System Plasma Physics, Vol. 3, Magnetic Field Reconnection*, ed. L. T. Lanzerotti, C. F. Kennel, & E. N. Parker (Amsterdam: North-Holland), 45
- Stawarz, J. E., Eastwood, J. P., Phan, T. D., et al. 2019, [ApJL](#), **877**, L37
- Sweet, P. A. 1958, in *IAU Symp. 6, Electromagnetic Phenomena in Cosmical Physics*, ed. B. Lehnert (Cambridge: Cambridge Univ. Press), 123
- Vega, C., Roytershteyn, V., Delzanno, G. L., & Boldyrev, S. 2020, [ApJL](#), **893**, L10
- Wang, R. S., Lu, Q. M., Lu, S., et al. 2020, [GeoRL](#), **47**, e88761
- Wang, R. S., Lu, Q. M., Nakamura, R., et al. 2018, [GeoRL](#), **45**, 4542
- Wang, S., & Lu, Q. M. 2019, *Collisionless Magnetic Reconnection* (Beijing: Science Press)
- Yamada, M., Kulsrud, R., & Ji, H. 2010, [RvMP](#), **82**, 603
- Yoon, P. H., & Lui, A. T. Y. 2004, [JGRA](#), **109**, A11213